

Effects of different methods for estimating impervious surface cover on runoff estimation at catchment level

Frank Canters¹, Jarek Chormanski², Tim Van de Voorde¹ and Okke Batelaan²

1 Department of Geography, Vrije Universiteit Brussel
Pleinlaan 2, B-1050 Brussel, Belgium
Tel.: + 0032 2 629 3381; Fax: + 0032 2 6293378
fcanters@vub.ac.be, tvdvoord@vub.ac.be

2 Department of Hydrology and Hydraulic Engineering, Vrije Universiteit Brussel
Pleinlaan 2, B-1050 Brussel, Belgium
Tel.: + 0032 2 629 3039; Fax: + 0032 2 6293022
jchorman@vub.ac.be, batelaan@vub.ac.be

Abstract

One of the most obvious effects of urbanization is an increase of impervious surface cover. Surface imperviousness has an important impact on hydrology, stream water quality and ecology, and is often used as an overall indicator of the health status of urbanized watersheds. It has also been identified as one of the key factors in the occurrence of flash floods. This paper examines the impact of different methods for estimating impervious surface cover on the outcome of a distributed rainfall-runoff model for the upper catchment of the Woluwe River in the southeastern part of Brussels. The study shows that mapping of impervious surface distribution, using remotely sensed data, produces substantially different estimates of average imperviousness for different types of urban land use. Little difference is observed between results obtained with detailed impervious surface maps derived from high resolution satellite data and sub-pixel estimates of imperviousness derived from medium resolution data. This demonstrates that sub-pixel classification may be an interesting alternative for more expensive high resolution mapping of imperviousness for rainfall-runoff modeling at catchment level.

Keywords: impervious surfaces, runoff modeling, remote sensing, sub-pixel classification

1 Introduction

One of the most obvious effects of urban growth is an increase of soil sealing caused by the construction of roads, buildings, parking lots,... The presence of anthropogenic impervious surfaces leads to more surface runoff, which in turn increases the risk for water pollution and floods in the watershed, hampers the recharging of aquifers and boosts erosion (Schueler, 1994; Arnold and Gibbons, 1996). Furthermore, impervious surfaces are warmer than their natural surroundings. This may have a profound impact on the local climate and the temperature of surface water. Information on the spatial distribution of impervious surfaces is therefore very important in hydrological modeling and is also increasingly used as a key indicator for the ecological condition of a watershed (Arnold and Gibbons, 1996; Sleavin *et al.*, 2000).

Different methods have been proposed for impervious surface mapping, many of which rely on existing land-use data sets (Sleavin *et al.*, 2000). These so-called indirect methods associate a percentage of imperviousness with each land-use type. The drawback of this approach is that

there is no standardized method for deriving these estimates and that there may be a high variability in the amount of imperviousness within the same land-use class. If mapping at a spatially more detailed level is required, a direct approach is preferred. Field inventorying and visual interpretation of large-scale, ortho-rectified aerial photographs are the most reliable methods to map impervious surfaces. However, because these methods are very time-consuming, they can in practice only be applied to relatively small areas. Satellite imagery, obtained from high resolution sensors like Ikonos or Quickbird, offers an interesting alternative for producing maps of surface imperviousness. Although high resolution imagery does not provide the same level of detail as large-scale aerial photographs, the use of automated or semi-automated image interpretation methods, exploiting the multi-spectral information content of the imagery, substantially reduces the effort that is required to produce reliable information on the distribution of impervious surfaces.

Despite the advantages of deriving impervious surface maps directly from high-resolution satellite imagery, the relatively limited footprint and price of such images pose difficulties if impervious surface maps are required for larger areas. A less expensive and more efficient alternative to map the spatial distribution of imperviousness in such cases is to develop models that allow estimation of the degree of imperviousness inside pixels of medium-resolution images (Landsat ETM+, ASTER,...). Over the past years, many sub-pixel regression and sub-pixel classification methods have been proposed that derive the proportion of impervious surfaces within a medium resolution pixel directly from the available multi-spectral data: multiple regression (Yang and Liu, 2005), spectral unmixing (Wu and Murray, 2003), neural networks (Wang and Zhang, 2004) and decision-trees (Huang and Townshend, 2003). Although the sub-pixel approach does not allow one to achieve the same degree of accuracy as when high-resolution data would be used, most studies report an average per pixel proportional error in the estimation of impervious surfaces of about 10%.

In this paper, a sub-pixel classification approach is presented for mapping the proportion of four major land-cover classes (impervious surfaces, vegetation, bare soil and water/shade), using both high and medium resolution satellite imagery. The approach involves two steps. First a land-cover map is produced from high resolution (HR) imagery covering part of the study area. The result is a spatially detailed land-cover map for a relatively small area, with a high level of accuracy. The HR classification is then used to train a sub-pixel classification model that estimates surface cover proportions within the pixels of a medium-resolution (MR) image covering a much larger area. The method was applied to Brussels and surroundings, using an Ikonos image that covers part of the city centre, the south-eastern suburbs of Brussels and the Sonian Forest, and an ETM+ image including the entire Brussels agglomeration. Land-cover class proportions derived from both the HR classification and the MR sub-pixel classification were used to characterize the distribution of land cover within the urban classes of an existing land-use map, produced by the Flemish Government, and used by regional and local authorities and research institutions within the region. The “land-cover enhanced” versions of the land-use map were used as input for a rainfall-runoff simulation on the upper catchment of the Woluwe River, located in the southeastern part of Brussels. The effect of different methods for characterizing urban land cover on estimated peak discharges was examined. Also the results obtained with HR and MR land-cover data were compared.

2 Methods

2.1 High-resolution land-cover mapping

To produce a high-resolution land-cover map of the study area, an Ikonos image of June 8, 2000 covering the southeastern part of Brussels was used. The image was registered to the Belgian Lambert coordinate system and orthorectified with a DEM available for Brussels. Applying a neural network classification approach, 11 land-cover classes were distinguished: light and dark red surfaces, light, medium and dark grey surfaces, bare soil, water, crops, shrub and trees, grass and shadows. Training data for the classification were obtained by digitizing about 200 randomly chosen training samples for each class. Different classification scenarios were tested, using various combinations of input variables: only the multi-spectral bands, the multi-spectral bands with the PAN band, the multi-spectral bands with the PAN band and a vegetation index (NDVI), and the multi-spectral bands with PAN, NDVI and 2 texture measures (local variance, binary comparison matrix). Transformations of the input bands and a selection according to their relative contribution to the overall information content were accomplished with NeuralWorks Predict®. The transformed input variables that were retained in each scenario to actually perform the classification were chosen from a set of 5 mathematical transformations per original input band using a genetic-based variable selection algorithm embedded in the software. The accuracy and the spatial coherence of the classification was further improved by applying post-classification techniques to remove shadow, reduce structural noise and correct classification errors (Van de Voorde *et al.*, in press). Finally, the 11 classes in the land-cover map were aggregated to a single vegetation class (including shrub and trees, grass and crops), a single impervious class (including red and grey surfaces), water and bare soil.

2.2 Subpixel classification

A neural network approach was adopted to estimate the proportions of four major land-cover classes (impervious surfaces, vegetation, bare soil and water/shade) in each pixel of a Landsat ETM+ image subset of October 18, 1999, covering Brussels and surroundings. The ETM+ image was co-registered to the Ikonos image using the ETM+PAN-band, resulting in an RMS error of 5.78m. To train the sub-pixel classifier, the land-cover classification derived from the Ikonos image was spatially aggregated to produce reference proportions for the four major land-cover classes for each ETM+ pixel in the overlapping zone between the two images. Because the images are not of the same date, precautions had to be taken not to include pixels in the training and validation phase with different land cover in both images due to seasonal shifts (leaf condition, crop cycles,...) or due to a change in land use (e.g. transition from non-built to built area). Since urban areas are dominated by impervious surfaces and vegetation, most changes in the 8-month period between the acquisition dates of both images will be related to changes in the vegetation component of the pixels. Therefore, in order to detect anomalous pixels the ETM+ NDVI values of all pixels in the overlap with the Ikonos image were plotted against the mean NDVI value of the constituent Ikonos pixels, after converting the raw DN's for both images to at-satellite reflectance values. A strong linear relationship was observed between ETM+ NDVI values and Ikonos mean NDVI values. Pixels deviating significantly from the trend were considered as indicative of major changes in land cover and were not used for training and validation. Feature selection and neural network building were accomplished with NeuralWorks Predict® software, starting from a set of transformations of all multispectral bands (1-5, 7) and all possible ratios between these bands. The performance of the sub-pixel classifier was assessed by calculating per-class mean error (ME_C), as well as

mean absolute error (MAE_C). To assess the impact of cell aggregation on proportional accuracy, all error measures were calculated at the original 30m resolution, as well as after aggregation of proportions to 60m and 90m.

2.3 Rainfall-runoff modeling

For the rainfall-runoff simulations use was made of WetSpa, a grid-based distributed hydrological model for water and energy transfer between soil, plants and atmosphere, which was originally developed by Wang *et al.* (1996) and adopted for flood prediction for hourly time steps by De Smedt *et al.* (2000), and Liu *et al.* (2002). For each grid cell a vegetation, root, transmission and saturated zone is considered in the vertical direction. The hydrological processes parametrised in the model are: precipitation, interception, depression, surface runoff, infiltration, evapotranspiration, percolation, interflow and groundwater flow. The total water balance for a raster cell is composed of the water balance for the vegetated, bare soil, open water and impervious parts of each cell. This allows accounting for within-cell heterogeneity of land cover. A mixture of physical and empirical relationships is used to describe the hydrological processes in the model. Interception reduces the precipitation to net precipitation, which on the ground is separated into rainfall excess and infiltration. Rainfall excess is calculated using a moisture-related modified rational method with a potential runoff coefficient depending on the land cover, soil type, slope, magnitude of rainfall, and antecedent moisture content of the soil. The calculated rainfall excess fills the depression storage at the initial stage and runs off the land surface simultaneously as overland flow. The infiltrated part of the rainfall may stay as soil moisture in the root zone, move laterally as interflow or percolate as groundwater recharge depending on the moisture content of the soil. Both percolation and interflow are assumed to be gravity driven in the model. Percolation out of the root zone is determined by the hydraulic conductivity, which is dependent on the moisture content as a function of the soil pore size distribution index. Interflow is assumed to occur in the root zone after percolation and becomes significant only when the soil moisture is higher than field capacity. Darcy's law and a kinematic approximation are used to estimate the amount of interflow generated from each cell, in function of hydraulic conductivity, moisture content, slope, and root depth. The actual evapotranspiration from soil and plant is calculated for each grid cell using the relationship developed by Thornthwaite and Mather (1955) as a function of potential evapotranspiration, vegetation stage, and moisture content in the cell.

Runoff from different cells in the watershed is routed to the watershed outlet depending on flow velocity and wave damping coefficient by using the diffusive wave approximation method. Although the spatial variability of land use, soil and topographic properties within a watershed are considered in the model, the groundwater response is modelled on the sub-catchment scale. The groundwater outflow is added to the generated runoff to produce the total stream flow at the sub-watershed outlet. Time-dependent inputs to the model are precipitation and potential evapotranspiration. Model parameters such as interception and depression storage capacity, potential runoff coefficient, overland roughness coefficient, root depth, soil property parameters, average travel time to the outlet, dispersion coefficient, etc., are determined for each grid cell using ArcView lookup tables and a high resolution DEM, soil type and land-use maps. The main outputs of the model are river flow hydrographs, which can be defined for any location in the channel network, and spatially distributed hydrological characteristics, such as soil moisture, infiltration rates, groundwater recharge, surface water retention, runoff, etc.

3 Results

3.1 High-resolution land-cover mapping

The high-resolution classification of the Ikonos image was obtained by training and comparing several neural networks, using different combinations of input bands. The best performing network consisted of 9 inputs, 17 hidden nodes and 11 output nodes (i.e. the 11 land-cover classes). The input variables were mathematical transformations of the red, green and blue image bands, the NDVI and two texture measures, namely standard deviation and binary comparison matrix. The overall performance of this network on an independent validation set of 2243 pixels was characterized by a kappa index-of-agreement of 0.91.

Despite the relatively high numeric accuracy of the classification result, many problems such as shadow, structural clutter and classification errors remained. The first step in improving the classification was to remove the shadow pixels using a technique described in Van de Voorde *et al.* (in press). In this approach, pixels originally classified as shadow are assigned to the most likely land-cover class using a second neural network. This network models the relationship between the class activation levels assigned to the shadow pixel in the original classification and the actual type of land cover present beneath the shadow, based on a set of shadow training pixels for which the type of land cover is known. The second step of the post-classification enhancement consists of applying knowledge based rules to correct classification errors and reduce structural clutter. In total, 14 region-based rules were developed and applied on the land-cover classification after shadow removal (Van de Voorde *et al.*, in press). The kappa index, which was calculated on the same validation set, increased from 0.91 to 0.95 after post-classification.

The 10 remaining classes in the land-cover map were aggregated to four classes (impervious surfaces, vegetation, bare soil and water). Finally, the resulting map was spatially aggregated to cells of 30m resolution, corresponding to the pixels in the overlapping Landsat ETM+ image, by calculating the proportion of each major land-cover class within a 30m cell. Figure 1 (left) shows the proportion of impervious surfaces within 30m cells for the area covered by the Ikonos image, including the centre of Brussels and the Sonian Forest in the southeast. The proportion maps obtained for the four major land-cover classes were used as reference data for training and validating the results of sub-pixel classification described below.

3.2 Sub-pixel classification

A sample of 3288 ETM+ pixels was randomly selected within the area of overlap between the Ikonos and ETM+ image. For each of these samples the ETM+ NDVI and the average NDVI of the Ikonos pixels that are part of it were calculated, after conversion of raw DNs to at-satellite reflectance values. A clear relationship was observed between ETM+ NDVI values and Ikonos mean NDVI values ($R^2 = 0.78$). Pixels deviating significantly from the trend (more than 2 times the standard deviation of the residuals) were considered as outliers and were removed from the sample, as these pixels were considered as indicative of possible changes in land cover in the period between the acquisition dates of the two images. The remaining samples (3118) were used for training the sub-pixel classifier. As mentioned before, six multispectral bands (1-5, 7), as well as all unique ratios of these bands were used as input. Mathematical transformations of all these input variables were calculated by NeuralWare Predict. The variable selection algorithm embedded in the software was used to withhold the variables that contain meaningful information. The neural network that was obtained has 6

inputs, 9 hidden nodes, and 4 output nodes. The transformed input channels that were withheld by the variable selection include the following bands and band ratios: B7, B3/B4 (2 transforms), B3/B5, B3/B7, B4/B5. Application of the model to the part of the Landsat ETM+ image that overlaps the Ikonos image produces four proportion maps (impervious surfaces, vegetation, bare soil and water). Figure 1 (right) shows the proportion map obtained for impervious surfaces. A visual comparison with the reference map of impervious surfaces, derived from the Ikonos image (Figure 1, left), shows a good correspondance in the overall pattern of imperviousness, although the sub-pixel result is more generalised and includes less structural detail.

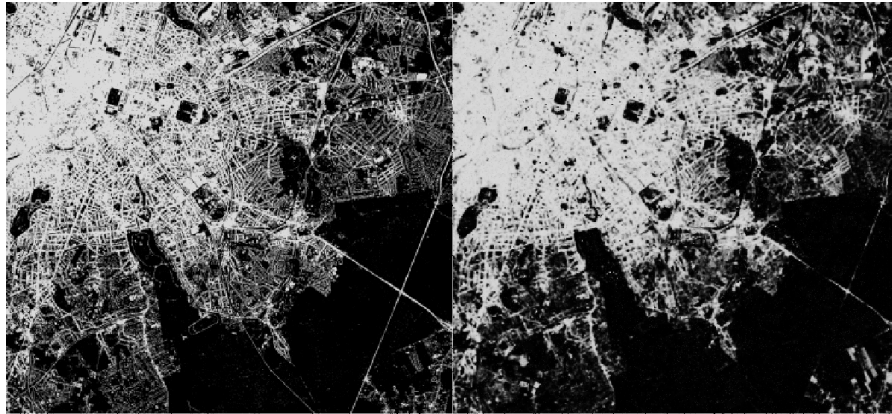


Figure 1. Maps of impervious surface proportion for the centre and southeast of Brussels, obtained by aggregation of an Ikonos-derived land-cover map to a cell size of 30m (left), and by sub-pixel classification of a Landsat ETM+ image (right). Light areas indicate high degrees of imperviousness.

Based on the trend equation used to remove outliers from the training sample, a mask of “unchanged” pixels was constructed covering the entire ETM+ image subset overlapping the Ikonos image. This mask was used for random selection of validation pixels, making sure that none of the training pixels was included in the validation sample. To assess the impact of cell aggregation on proportional accuracy, error measures were calculated at the original 30m resolution, as well as after aggregation of proportions to 60m and 90m. Two types of errors measures were utilized: per-class mean error (ME_C) and per-class mean absolute error (MAE_C). ME_C is simply the mean difference between estimated and reference proportions for all validation pixels in one class, and describes systematic error (over- or underestimation). MAE_C is the mean absolute difference between estimated and reference proportions and is a measure of estimation accuracy. Table 1 shows that impervious surfaces and bare soil are slightly underestimated, while vegetation and water are slightly overestimated. The slight underestimation of impervious surfaces (-1.8%) may be explained by the presence of shadow in urbanized areas. When examining the estimated proportion of water within the area, it turns out that small portions of many urban pixels are assigned to water, although no water is present within these pixels. This phenomenon is most clearly observed in dense urban areas and is most likely caused by the presence of shadow, which is spectrally similar to water. As such, the proportion of water identified by the sub-pixel estimator should better be interpreted as

water/shade, as it may point to the presence of both components. This may also explain the slight overestimation of water observed in Table 1 (+1.1%).

Table 1 also includes MAE_C values for all classes. As can be seen the mean absolute error for impervious surfaces and vegetation, which are the two dominant classes in the image, is around 10%. Aggregation to cell sizes of 60m and 90m reduces this error to 7.5% and 6.1% for impervious surfaces, and to 7.2% and 5.9% for vegetation. Residual analysis (Figure 2) indicates that the mean absolute error for impervious surfaces is the highest (up to 25% or more) for heterogeneous pixels, where the reference proportion is close to 50%. Pixels with high or low proportions of impervious surfaces (<10% or >90%) have much smaller errors (between 5% and 10%). Aggregation to cell sizes of 60m and 90m substantially reduces proportional errors, especially for pixels with a strongly mixed class composition. As a result of aggregation, the peak value in the graph, indicating which reference proportions have the highest proportional error, seems to shift to lower proportions for impervious surfaces (Figure 2) and to higher proportions for vegetation. For cell sizes of 90m the average proportional error is the highest for pixels with around 30% impervious surfaces and around 70% vegetation.

Table 1. Mean error (ME_C) and mean absolute error (MAE_C) for the four major land-cover classes for cell sizes of 30m, 60m and 90m.

Cell size	Mean error				Mean absolute error			
	Impervious	Vegetation	Bare soil	Water	Impervious	Vegetation	Bare soil	Water
30m	-0.018	0.015	-0.049	0.011	0.1030	0.1017	0.0593	0.0166
60m	-0.017	0.014	-0.048	0.011	0.0752	0.0720	0.0514	0.0152
90m	-0.019	0.015	-0.045	0.011	0.0611	0.0590	0.0467	0.0153

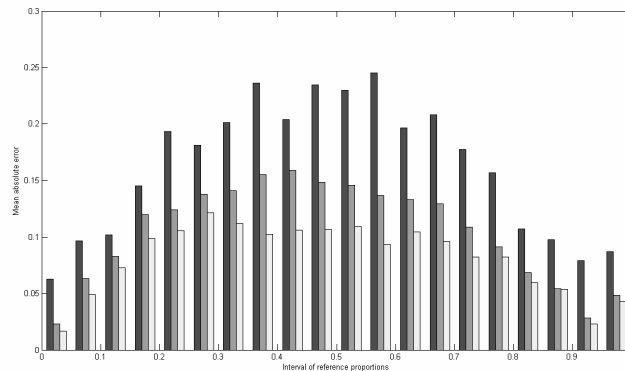


Figure 2. Mean absolute error (MAE_C) for impervious surfaces for different intervals of reference proportions.

3.3 Rainfall-runoff modeling

Three alternative land-cover scenarios were tested: one in which a single impervious surface coefficient is defined for all urban land-use classes, a second where separate coefficients are

derived for different types of urban land use, and finally, a spatially fully distributed scenario where each urban cell is assigned its own set of land-cover proportions.

3.3.1 Scenario 1

The first scenario corresponds to a situation, which often occurs in hydrology: the case where no information is available about different types of land use within the urban area, nor about the distribution of impervious surfaces within the urban zone. To simulate run-off for this scenario all classes in the Flemish land-use map were aggregated to one non-differentiated urban class. Next, according to the WetSpa default values, 30% of all the cells in the urban area was assumed to be impervious, with the remaining part of the cells assigned to grass. This basic scenario was improved by using the proportion maps, derived from the Ikonos land-cover classification and from the sub-pixel classification of Landsat data, to estimate the average percentage of imperviousness for urban area in a less arbitrary way. The values for average imperviousness obtained with Ikonos and Landsat proved to be very similar (44% and 46% respectively), but substantially differ from the default value (30%). Simulating runoff for different degrees of imperviousness shows that peak discharges are very sensitive to the presence of impervious surfaces in urbanized watersheds (Figure 3). Remote sensing data are a valuable source for obtaining a realistic estimate of the average degree of imperviousness. The estimated peak discharges for an average degree of imperviousness of 44% (Ikonos estimate) prove to be 10-20% higher than in the default scenario.

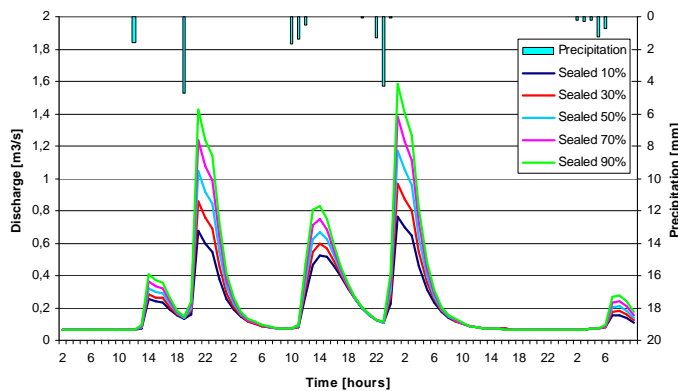


Figure 3. Comparison of hydrographs for different degrees of imperviousness (simulation period 3rd of May 2005, 1.00 am till 6th of May 2005, 9.00 am).

3.3.2 Scenario 2

In this scenario, each of the 6 built-up classes in the land-use map of Flanders was assigned a different level of imperviousness based on the Ikonos- and Landsat-derived proportion maps. The average degree of imperviousness for different land-use classes obtained from Ikonos and Landsat data are quite similar (Table 2). For some classes, however, the values derived from the proportion maps strongly differ from default values obtained from the literature. This again demonstrates the benefit of using remotely sensed data for obtaining estimates of average

degrees of imperviousness. Use of class-specific degrees of imperviousness produced slightly higher peak discharges than the use of one average value for the entire built-up area.

Table 2. Degree of imperviousness for different urban land-use classes: default values and estimates derived from Ikonos data and Landsat data.

Land-use class	Default degree of imperviousness	Ikonos-derived value	Landsat-derived value
Low density built-up	0.30	0.12	0.12
High density built-up	0.50	0.57	0.61
City centre	0.70	0.45	0.38
Infrastructure	0.50	0.58	0.60
Roads	0.50	0.36	0.31
Industry	0.70	0.84	0.86

3.3.3 Scenario 3

Finally, a fully distributed scenario was applied, where each cell in the urban area is assigned its own proportion of impervious surface, vegetation, bare soil and water, as obtained from the Ikonos- and Landsat-derived proportion maps. Analysing and comparing the results for the 3 scenarios, the runoff calculated in scenario 3, and based on the Ikonos data, produces the highest peak discharges. The peaks are about 10% higher than in scenario 1. Using information about the spatial distribution of imperviousness within urban areas seems to have a clear impact on the modelling of peak discharges at the outlet of the catchment and, therefore, on flood prediction. The hydrograph simulated in scenario 3, but based on Landsat data, has slightly lower peaks than the one based on Ikonos, yet both hydrographs are very alike. This proves that sub-pixel classification of Landsat data may be an interesting alternative for expensive high-resolution mapping, especially if one wants to work on larger areas. The spatial differentiation in runoff is obvious from the map of runoff coefficients obtained for scenario 3 (Figure 4). High values for runoff coefficients, in the range of 0.8-1.0, prove to be linked to a closely connected pattern of impervious areas.

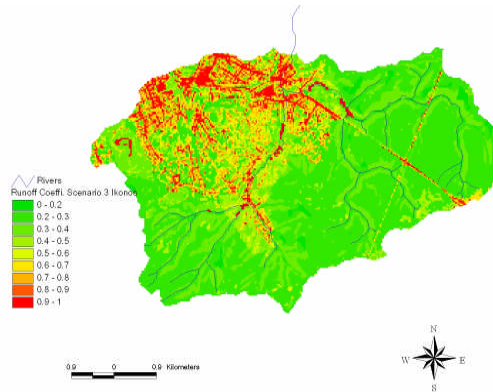


Figure 4. Map of runoff coefficients for scenario 3, based on Ikonos-derived land-cover data.

4 Conclusions

The study shows that estimates of average imperviousness derived from satellite data may strongly differ from expert knowledge for some urban land-use classes, leading to substantially different estimates of discharge at catchment level. Furthermore, the use of spatially distributed land-cover information obtained from satellite derived maps proves to produce higher peak discharges compared to scenarios based on the use of average levels of imperviousness for each land-use class. Little difference was observed between results obtained with detailed impervious surface maps derived from high resolution data and with sub-pixel estimates of imperviousness derived from MR data. This proves that multi-resolution methods, which provide information on surface imperviousness for areas of large extent at relatively low cost, may be an interesting alternative for expensive high resolution mapping for rainfall-runoff modelling at catchment level.

Acknowledgements

The authors wish to express their gratitude to Tim De Roeck of the Department of Geography of the Vrije Universiteit Brussel for his part in the work on impervious surface mapping. Belgian Science Policy is gratefully acknowledged for providing the funds for this research. The second author also acknowledges the support of the Research in Brussels programme for a post-doctoral fellowship.

References

- Arnold, C.A. Jr. and Gibbons, C.J., 1996, Impervious surface coverage: the emergence of a key urban environmental indicator. *Journal of the American Planning Association*, 62 (2), pp. 243-258.
- De Smedt, F., Liu, Y.B. and Gebremeskel, S., 2000, Hydrologic modeling on a catchment scale using GIS and remote sensed land use information. In *Risk Analysis II*, C.A. Brebbia (Ed.), pp. 295-304, Southampton, Boston: WIT Press.
- Huang, C. and Townshend, J.R.G., 2003, A stepwise regression tree for nonlinear approximation: applications to estimating subpixel land cover. *International Journal of Remote Sensing*, 24 (1), pp. 75-90.
- Liu, Y.B., De Smedt, F. and Pfister, L., 2002, Flood prediction with the WetSpa model on catchment scale. In *Flood Defence 2002*, Wu *et al.* (Eds.), pp. 499-507, New York: Science Press Ltd.
- Schueler, T.R., 1994, The importance of imperviousness. *Watershed Protection Techniques*, 1 (3), pp. 100-110.
- Sleavin, W.J., Civco, D.L., Prisløe, S. and Gianotti, L., 2000, Measuring impervious surfaces for nonpoint source pollution modeling. In *Proceedings of the ASPRS 2000 Annual Conference*, Washington, DC, unpaginated CD-ROM.
- Thorntwaite, C. W. and Mather, J. R., 1955, The water balance. *Laboratory of Climatology, Publ. No. 8, Centerton NJ*.
- Van de Voorde, T., De Genst, W. and Canters, F., (in press), Improving pixel-based VHR land-cover classifications of urban areas with post-classification techniques. *Photogrammetric Engineering and Remote Sensing*.
- Wang, Y. and Zhang, X., 2004, A SPLIT model for extraction of subpixel impervious surface information. *Photogrammetric Engineering and Remote Sensing*, 70 (7), pp. 821-828.
- Wang, Z., Batelaan, O. and De Smedt, F., 1996, A distributed model for Water and Energy Transfer between Soil, Plants and Atmosphere, *Phys. Chem. Earth*, 21 (3), pp. 189-193.
- Wu, C. and Murray, A.T., 2003, Estimating impervious surface distribution by spectral mixture analysis. *Remote Sensing of Environment*, 84, pp. 493-505.
- Yang, X. and Liu, Z., 2005, Use of satellite-derived landscape imperviousness index to characterize urban spatial growth. *Computers, Environment and Urban Systems*, 29, pp. 524-540.